ICOSSAR 2021
The 13th International Conference on Structural Safety and Reliability (ICOSSAR 2021-2022), September 13-17, 2022, Shanghai, P.R. China
J. Li, Pol D. Spanos, J.B. Chen & Y.B. Peng (Eds)

Multi-fidelity surrogate model for efficient tsunami evacuation risk assessment

Min Li[a], Zhenqiang Wang[a], and Gaofeng Jia[a]

[a]*Department of Civil and Environmental Engineering, Colorado State University, Fort Collins, CO, USA. E-mail: Min.Li@colostate.edu; Zhenqiang.Wang@colostate.edu; Gaofeng.Jia@colostate.edu.*

ABSTRACT: For coastal communities subjected to tsunami hazard, to guide risk-informed evacuation planning, it is critical to accurately assess the evacuation risk. To simulate the evacuation process, agent based models (ABM) have been used. However, ABM is typically quite expensive to run, especially when the number of agents/evacuees is large. Direct adoption of such model in evacuation risk assessment entails significant computational challenges. To address this, this paper develops multi-fidelity Gaussian process (MFGP) model to replace the high-fidelity ABM model for efficient evacuation risk assessment. MFGP model is trained using small number of runs of high-fidelity ABM model and large number of cheaper lower-fidelity ABM models established using simplified assumptions. Principal component analysis (PCA) is used to reduce the dimension of the temporal and spatial outputs related to evacuation, and the MFGP model is trained efficiently for the low-dimensional latent outputs. Application to tsunami evacuation risk assessment for Seaside, Oregon verifies the high accuracy and efficiency of the MFGP.

1 INTRODUCTION

An earthquake-induced tsunami can cause significant loss of life, especially for the low-lying coastal communities facing the near-field tsunami strike. Evacuation to safety zones is regarded as the most effective way to survive a tsunami. To provide valuable information for effective evacuation planning, the tsunami evacuation risk needs to be assessed.

To accurately assess the tsunami evacuation risk, the complex evacuation process needs to be modeled and various uncertainties in the evacuation need to be quantified and propagated. Recently, agent-based modeling (ABM) has been used to simulate the evacuation process considering its capability of capturing the emergent phenomenon, providing a natural description of the evacuation system, and being flexible (Bonabeau, 2002; Wang et al., 2016; Wang and Jia, 2021). However, the high-fidelity agent-based model is typically quite expensive to run when fully characterizing the natural and human system dynamics and modeling the realistic evacuation behaviors, individual-level interactions among agents, and the agents' interactions with the multi-hazard environment. To assess the evacuation risk, various uncertainties associated with the evacuation need to be quantified and propagated including those associated with the multiple hazards (i.e., cascading hazards of earthquake and tsunami) and the evacuation decisions and behaviors. Direct adoption of high-fidelity ABM model in stochastic simulation based uncertainty propagation to estimate evacuation risk entails significant computational challenges.

ICOSSAR 2021
The 13th International Conference on Structural Safety and Reliability (ICOSSAR 2021-2022), September 13-17, 2022, Shanghai, P.R. China
J. Li, Pol D. Spanos, J.B. Chen & Y.B. Peng (Eds)

To facilitate efficient risk assessment and uncertainty quantification in general, in the literature, surrogate models have been proposed to replace the expensive system models (Dubourg et al., 2011; Jia and Taflanidis, 2013; Gidaris et al., 2015; Jia et al., 2016). To build surrogate models, high-fidelity training data are needed. For expensive models, the total number of high-fidelity training data may be limited, which may lead to low accuracy of trained surrogate model. To efficiently build surrogate models with high accuracy, multi-fidelity surrogate models have been proposed, which can leverage the trend information provided by a large number of low-fidelity model runs (i.e., less accurate but cheap to establish) and the accuracy provided by a small number of expensive high-fidelity model runs (i.e., accurate but expensive to establish) (Kennedy and O'Hagan, 2000; Qian et al., 2006; Li and Jia, 2020).

Inspired by the metamodeling approach developed in Gidaris et al. (2015) for seismic risk assessment, we develop surrogate models for efficient tsunami evacuation risk assessment. In Gidaris et al. (2015), kriging surrogate model is trained based on high-fidelity data to approximate the relationship between the structural response and the structural and ground motion parameters that are considered as uncertain, where to address the stochastic character of the seismic excitation under the influence of the white noise surrogate model is built with respect to the statistics of the structural responses under different realizations of the white noise.

Here, instead of kriging metamodel trained on only high-fidelity data, this paper develops multi-fidelity Gaussian process (GP) surrogate model to replace the high-fidelity ABM model for efficient evacuation risk assessment. Besides high-fidelity ABM model, cheaper lower-fidelity ABM model is established by using simplified assumptions (e.g., constant evacuation speed, larger time steps, and smaller population size). Then an accurate MFGP surrogate model is trained by using the multi-fidelity training data. In addition, to address the challenge of high dimensional outputs (e.g., the spatial and temporal evacuation performances), principal component analysis (PCA) is used to reduce the output dimension and establish low dimensional latent outputs. MFGP model is then efficiently trained with respect to the latent outputs. In the end, the MFGP model is used to efficiently evaluate the tsunami evacuation risk for Seaside, Oregon, and the impacts of population size and evacuation behaviors on the evacuation risk are investigated.

2 QUANTIFICATION OF TSUNAMI EVACUATION RISK

2.1 *Tsunami evacuation risk*

To quantify the tsunami evacuation risk, we use the simulation-based framework shown in Fig. 1. In particular, $\mathbf{x} = [x_1, \ldots, x_i, \ldots, x_{n_x}] \in X$ represents the inputs into the tsunami evacuation model and $\xi = [\xi_1, \ldots, \xi_i, \ldots, \xi_{n_\xi}] \in \Xi$ represents the uncertain model parameters in the evacuation model, and $y(\mathbf{x}, \xi)$ represents the evacuation performances (e.g., the casualty rate) for given $[\mathbf{x}, \xi]$. We use the probability distribution function (PDF) $p(\xi|\mathbf{x})$ to quantify the uncertainty in ξ under given $\mathbf{x}$. $h(\mathbf{x})$ represents the risk consequence measure for given $\mathbf{x}$. Propagating the uncertainties in $\mathbf{x}$, quantified by PDF $p(\mathbf{x})$, leads to the quantification of the evacuation risk (denoted H)

$$H = \int_X h(\mathbf{x}) p(\mathbf{x}) \mathrm{d}\mathbf{x} \tag{1}$$

For given input $\mathbf{x}$, to calculate the risk consequence measure $h(\mathbf{x})$, the uncertainties in the evacuation model need to be considered. Typically, $h(\mathbf{x})$ is related to the distribution or statistics of the evacuation performance $y(\mathbf{x}, \xi)$. For example, $h(\mathbf{x})$ can be probability of $y(\mathbf{x}, \xi)$ exceeding certain threshold and this probability can be established using the distribution information (e.g., mean and standard deviation in case of normal or lognormal distribution) of $y(\mathbf{x}, \xi)$ (Gidaris et al., 2015). To

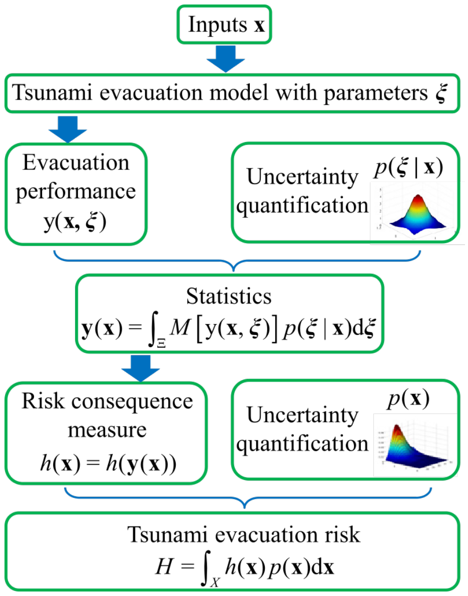

Figure 1. Framework for quantification of tsunami evacuation risk.

this end, we use $\mathbf{y}(\mathbf{x})$ to represent the statistics (e.g., mean and/or standard deviation) of $y(\mathbf{x}, \xi)$. In this context, $\mathbf{y}(\mathbf{x})$ can be written in more general form as

$$\mathbf{y}(\mathbf{x}) = \int_\Xi M[y(\mathbf{x}, \xi)] p(\xi | \mathbf{x}) d\xi \tag{2}$$

where $M[.]$ is a function such that Eq. (2) gives the interested statistics $\mathbf{y}(\mathbf{x})$. Essentially, $h(\mathbf{x})$ can be written as $h(\mathbf{x}) = h(\mathbf{y}(\mathbf{x}))$. Later in the illustrative example, we focus on the mean of $y(\mathbf{x}, \xi)$, in which case $M[y(\mathbf{x}, \xi)] = y(\mathbf{x}, \xi)$.

Note that in the context of evacuation risk assessment, since many times we are interested in the spatial and temporal evacuation performance, the output $y(\mathbf{x}, \xi)$ and corresponding $\mathbf{y}(\mathbf{x})$ could be high-dimensional. For $\mathbf{y}(\mathbf{x})$, it can be written as $\mathbf{y}(\mathbf{x}) = [y_1(\mathbf{x}), ..., y_{n_y}(\mathbf{x})]$ with dimension of n_y.

2.2 *Conditional tsunami evacuation risk*

Besides the evacuation risk, we are also interested in investigating how the evacuation risk varies with the critical model inputs. Some inputs in $\mathbf{x}$ might have larger impacts on the evacuation risk (i.e., critical model inputs such as the proportion of the population that evacuate by car in the multi-modal evacuation) than others. Such investigations can provide importation information for effective evacuation planning. For this, we need to evaluate the so-called conditional evacuation risk. For example, if we are interested in the impact of input x_i, then we can define conditional evacuation risk $H(x_i)$, which represents the conditional evacuation risk under the given value of x_i and can be quantified by

$$H(x_i) = \int_{X_{\sim i}} h(\mathbf{x}_{\sim i}, x_i) p(\mathbf{x}_{\sim i}) d\mathbf{x}_{\sim i} \tag{3}$$

where $\mathbf{x}_{\sim i}$ represents the remaining of the inputs excluding x_i. Besides scalar input x_i, the evacuation risk conditional on any subsets of $\mathbf{x}$, denoted $\mathbf{x}_s$ (with $\mathbf{x}_s \subset \mathbf{x}$), can be defined similarly.

2.3 *Computational challenges*

To estimate the evacuation risk H in Eq. (1), general stochastic simulation techniques such as Monte Carlo Simulation (MCS) can be used. However, it typically requires a large number of evaluations of $h(\mathbf{x})$. In the context of the current problem, each evaluation of $h(\mathbf{x})$ would require calculation of $\mathbf{y}(\mathbf{x})$ that involves propagating uncertainties in ξ based on Eq. (2) and is quite expensive itself due to the need to repeatedly run the evacuation model. Overall, evaluation of the evacuation risk H entails significant computational challenges. It would be even more computationally expensive to estimate the conditional evacuation risk (e.g., $H(x_i)$) due to the need to repeat the evacuation risk estimation for different values of x_i (or more generally $\mathbf{x}_s$).

3 RISK ASSESSMENT USING MULTI-FIDELITY GAUSSIAN PROCESS MODEL

This section presents the proposed approach for efficient evacuation risk assessment using multi-fidelity Gaussian process (GP) surrogate model.

3.1 *Multi-fidelity Gaussian Process model with PCA*

The development of the multi-fidelity Gaussian process model requires, first, the creation of a high-fidelity database (i.e., n_h simulations based on the high-fidelity numerical model for input $\mathbf{X}_h = \{\mathbf{x}_h^1, \ldots, \mathbf{x}_h^{n_h}\}$) and a low-fidelity database (i.e., n_l simulations based on the low-fidelity numerical model for input $\mathbf{X}_l = \{\mathbf{x}_l^1, \ldots, \mathbf{x}_l^{n_l}\}$). The selection of these inputs is frequently referenced as design of experiments, and can be established using some space filling technique such as Latin Hypercube Sampling (LHS). These selected input points are also frequently referenced as the *training set* or *support points*. It is noteworthy to point out that here X_h is taken as a subset of $\mathbf{X}_l$, which allows direct comparison between high-fidelity data and low-fidelity data for the design sites in $\mathbf{X}_h$, guiding how the low-fidelity data should be "corrected" to match the high-fidelity data.

Let $\mathbf{Y}_l$ of size $n_l \times n_y$ denote the observation matrix from the low-fidelity model (i.e., response over $\mathbf{X}_l$), and $\mathbf{Y}_h$ of size $n_h \times n_y$ the observation matrix from the high-fidelity model (i.e., response over $\mathbf{X}_h$). Let $\mathbf{Y} = [\mathbf{Y}_l; \mathbf{Y}_h]$ denote the joint observation matrix, which has size $n \times n_y$ with $n = n_l + n_h$. Considering the fact that there are differences between the low-fidelity outputs and the high-fidelity outputs, the outputs $\mathbf{Y}_l$ and $\mathbf{Y}_h$ should be normalized before combining them.

We then apply PCA to $\mathbf{Y}$ to find a low-dimensional representation. Based on $\mathbf{Y}$, we can establish a transformation

$$\mathbf{Y}^T = \mathbf{P}\mathbf{Z}^T \tag{4}$$

where $\mathbf{P}$ is the $n_y \times n_z$ projection matrix containing the eigenvectors corresponding to the n_z largest eigenvalues, and $\mathbf{Z}$ is the latent output matrix that has size of $n \times n_z$. Note that in Eq. (4), there is an truncation error that is typically very small, and not explicitly written. In $\mathbf{Z}$, we can identify the latent output that correspond to the low-fidelity outputs and high-fidelity outputs, denoted as $\mathbf{Z}_l$ and $\mathbf{Z}_h$, respectively. $\mathbf{Z} = [\mathbf{Z}_l; \mathbf{Z}_h]$, with $\mathbf{Z}_l$ having size of $n_l \times n_z$ and $\mathbf{Z}_h$ having size of $n_h \times n_z$.

Based on $\mathbf{Z}_l$ and $\mathbf{Z}_h$, we then train multi-fidelity Gaussian process (MFGP) model for the latent outputs

$$\mathbf{z}_h(\mathbf{x}) = \rho\mathbf{z}_l(\mathbf{x}) + \mathbf{z}_\delta(\mathbf{x}) \tag{5}$$

Once the surrogate model is established in the latent spaces for $\mathbf{z}_l(\mathbf{x})$ and $\mathbf{z}_\delta(\mathbf{x})$, denoted as $\hat{\mathbf{z}}_l(\mathbf{x})$ and $\hat{\mathbf{z}}_\delta(\mathbf{x})$, the prediction for $\mathbf{z}_h(\mathbf{x})$ can be established as $\hat{\mathbf{z}}_h(\mathbf{x}) = \rho\hat{\mathbf{z}}_l(\mathbf{x}) + \hat{\mathbf{z}}_\delta(\mathbf{x})$. Then the prediction for the original output can be established through the transformation

$$\hat{\mathbf{y}}_h(\mathbf{x}) = \mathbf{P}\hat{\mathbf{z}}_h(\mathbf{x}) = \mathbf{P}\left[\rho\hat{\mathbf{z}}_l(\mathbf{x}) + \hat{\mathbf{z}}_\delta(\mathbf{x})\right] \tag{6}$$

Overall, instead of building multi-fidelity Gaussian process in the original output space, we first build multi-fidelity Gaussian process for the low-dimensional latent outputs with the formulation in Eq. (5) and then for prediction at new input $\mathbf{x}$, first the established MFGP is used to predict the latent outputs, then the PCA transformation in Eq. (6) is used to directly transform the latent outputs to the corresponding outputs in the original space.

To evaluate the accuracy of the established MFGP, error statistics are calculated using leave-one-out cross validation (LOOCV), which is performed as follows. First, the observations from the high-fidelity data set is sequentially removed, and the corresponding training data set will be composed of the remaining high-fidelity data and the original low-fidelity data. Second, the MFGP is trained based on the corresponding training set and used to predict the response over the removed data point. Finally, for the high-fidelity data points, there is an observation matrix and a prediction matrix, both of which are of size $n_h \times n_y$). Based on the matrices, the error between the predictions and the high-fidelity observations (i.e., the overall LOOCV error) can be calculated. Here we use the mean error *ME* as the error statistics, and the LOOCV *ME* is given by:

$ME = \sum_{i=1}^{n_h} |\mathbf{y}_h(\mathbf{x}_h^i) - \hat{\mathbf{y}}_h(\mathbf{x}_h^i)| / \sum_{i=1}^{n_h} |\mathbf{y}_h(\mathbf{x}_h^i)|$, where $\hat{\mathbf{y}}_h(\mathbf{x}_h^i)$ is the mean prediction from the established MFGP. Smaller value for ME means better accuracy of the trained MFGP.

Due to the high computational effort for each evaluation of the high-fidelity model, it is desirable to use small number for n_h, but at the same time we want the MFGP model to have good accuracy. To select an appropriate n_h and n_l, we investigate how the ME changes over different selection of n_h and n_l. When there is little variation in ME or when ME is below a target level, indicating good accuracy of the established MFGP model, we select the corresponding n_h and n_l values. Here to establish the training data, LHS is used to sample evenly in the input space, so that the trained MFGP will have good accuracy over the input space. The training data (especially the high-fidelity data) can also be adaptively selected based on criteria such as the variance of the GP model to effectively build MFGP model with high accuracy. This will be explored in future research.

3.2 *Risk estimation using MFGP*

Then the trained MFGP is used to predict the risk consequence measure $h(\mathbf{x}) = h[\hat{\mathbf{y}}_h(\mathbf{x})]$ for any given $\mathbf{x}$ for efficient risk estimation. The evacuation risk H is estimated using MFGP with N simulations by

$$\hat{H} = \frac{1}{N} \sum_{k=1}^{N} h[\hat{\mathbf{y}}_h(\mathbf{x}^k)] \tag{7}$$

where $\mathbf{x}^k$ is the k^{th} sample of the input $\mathbf{x}$ generated from $p(\mathbf{x})$. The high efficiency of MFGP means that a larger N value can be used to improve the accuracy of the risk estimate. Similarly, the conditional evacuation risk (e.g., $H(x_i)$) can be estimated

$$\hat{H}(x_i) = \frac{1}{N} \sum_{k=1}^{N} h[\hat{\mathbf{y}}_h(\mathbf{x}_{\sim i}^k, x_i)] \tag{8}$$

4 ILLUSTRATIVE EXAMPLE

4.1 *Study area*

We select Seaside, Oregon (shown in Fig.2(b)) as the study area for the tsunami evacuation risk assessment. Seaside is located close to the Cascadia Subduction Zone (CSZ, shown in Fig.2(a)), which makes the community have a high risk to the combined CSZ seismic and tsunami hazard, and many tsunami evacuation studies have been focused on this community (Wang et al., 2016; Mostafizi et al., 2017, 2019).

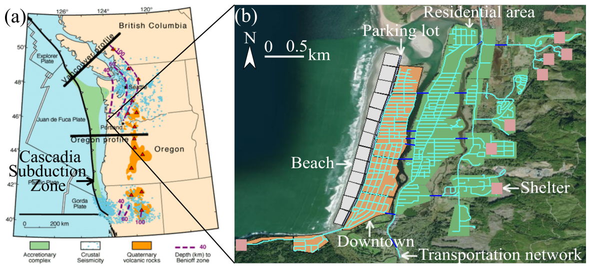

Figure 2. (a) Cascadia Subduction Zone (CSZ) (USGS, 2020), and (b) Seaside, Oregon.

4.2 *Agent-based tsunami evacuation model*

4.2.1 *High-fidelity model*

We adopt the agent-based model for tsunami evacuation simulation developed in Wang (2021) as the high-fidelity agent-based tsunami evacuation model. The agent-based model in Wang (2021) is developed through improving the agent-based tsunami evacuation model introduced in Wang and Jia (2021), which extends on the agent-based modeling framework for near-field tsunami evacuation proposed in Wang et al. (2016). The model used here is briefly reviewed.

The agent-based tsunami evacuation model consists of the evacuation environment model (EEM), evacuation decision and behavior model (EBM), and evacuation performance model (EPM). The EEM includes the multi-hazard model (i.e., seismic and tsunami hazards), transportation network, tsunami shelter, and population distribution. The traffic capacity reductions of the damaged bridge due to the seismic damage and the blocked road due to debris from damaged buildings are considered. The time histories of the tsunami inundation are generated using ComMIT/MOST. In the EBM, the evacuation decision and behavior are modeled. The evacuation decision includes the departure time, the multi-modal evacuation (i.e., evacuation on foot and by car), and the path selection such as searching the shortest path. For the evacuation behavior, individual behavior and interactions between evacuees and with the damaged environment are modeled. The speed adjustment for both the pedestrian and car is considered in the modeling of the individual evacuation behavior. The interactions between evacuees include those occurring between pedestrians or cars (e.g., following others), and between the pedestrian and car (e.g., the pedestrian-vehicle interaction modeled by the traffic stage transition). The interactions between evacuees and the damaged environment include the traffic capacity reduction of the damaged bridge or blocked road, reroute behavior (e.g., when traffic jam occurs ahead), and acceleration behavior for pedestrians (e.g., when inundation comes closer). In the EPM, the commonly used quantity of interest such as the casualty rate can be selected as the evacuation performance measure and the critical water depth is used to determine the casualty.

The agent-based tsunami evacuation model is developed in NetLogo. Fig. 3 shows the developed model, where (a) shows a realization of the population distribution in the study area and (b) shows the evacuation at a certain time instant. Due to the incorporation of many important factors and mechanisms associated with the evacuation process and the detailed modeling, the high-fidelity model is quite expensive to run.

4.2.2 *Low-fidelity model*

Based on the high-fidelity agent-based tsunami evacuation model, the low-fidelity evacuation model is developed by neglecting the pedestrian-vehicle interaction and the

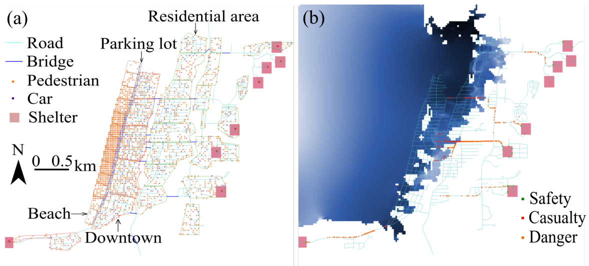

Figure 3. Illustration of the high-fidelity agent-based tsunami evacuation model.

speed adjustment for both the pedestrian and car in the EBM. When the pedestrian-vehicle interaction is neglected, the pedestrian and car travel on the sidewalk and lane with the fixed width, respectively (i.e., corresponding to the balanced traffic stage in the simulation of the pedestrian-vehicle interaction (Wang and Jia, 2021)). Also, the pedestrian evacuates at the preferred walking speed and the car drives at the free-flow speed. Compared to the high-fidelity evacuation model, the low-fidelity model is cheaper to run but with lower accuracy.

4.3 *Implementation details*

4.3.1 *High-fidelity model*

We consider the historical seismic event in 1700 as the hypothetical seismic and tsunami hazard inputs, in which $M_w = 9.0$ and the focal depth of 40 km are considered. It is assumed that the tsunami evacuation occurs at noontime of some weekend in summer and lasts for one hour starting the occurrence of the earthquake.

For the high-fidelity model described in the previous section, it is implemented in NetLogo with a time step of five seconds. Table 1 summarizes the model parameters ξ and associated uncertainties in the context of the evacuation risk quantification described in Section 2, in which "U" represents the uniform distribution on the interval given in the parentheses. The departure time t (unit: min) follows Rayleigh distribution with delay time τ (unit: min) and scalar parameter σ_t. Both τ and σ_t are parts of the inputs $\mathbf{x}$, which are defined in Table 2. The pedestrian speed v_p

ICOSSAR 2021
The 13th International Conference on Structural Safety and Reliability (ICOSSAR 2021-2022), September 13-17, 2022, Shanghai, P.R. China
J. Li, Pol D. Spanos, J.B. Chen & Y.B. Peng (Eds)

Table 1. Model parameters ξ in the tsunami evacuation simulation using the high-fidelity agent-based model.

ξ_i	Distribution
t	Rayleigh distribution with delay time τ and scalar parameter σ_t
v_p	Normal distribution with mean μ_p and SD σ_p, truncated in (0.75, 3.83)
$T_{1_{PA}}$; $T_{2_{PA}}$	$U(1.00, 1.53)$; $U(2.30, 4.19)$
$T_{1_{MA}}$; $T_{2_{MA}}$	$U(0.59, 0.97)$; $U(1.64, 3.14)$
$T_{1_{Mac}}$; $T_{2_{Mac}}$	$U(0.59, 0.97)$; $U(1.53, 2.79)$
$T_{1_{LR}}$; $T_{2_{LR}}$	$U(0.27, 0.38)$; $U(0.54, 1.04)$

follows truncated in (0.75, 3.83) (unit: m/s) normal distribution with mean μ_p (unit: m/s) and standard deviation (SD) σ_p (unit: m/s). Both μ_p and σ_p are included in the inputs **x**. $T_{1_{PA}}$, $T_{2_{PA}}$, $T_{1_{MA}}$, $T_{2_{MA}}$, $T_{1_{Mac}}$, $T_{2_{Mac}}$, $T_{1_{LR}}$, and $T_{2_{LR}}$ represents the threshold in the traffic stage transition and corresponds to the road class "Principle Arterial", "Minor Arterial", "Major Collector", and "Local Road", respectively. In addition, ξ includes the parameters associated with seismic damages to bridges and buildings (e.g., the seismic damage state DS_j with $j = 1,2,\ldots 5$), and the parameters associated with the location of the population.

Table 2 presents the inputs **x** for the high-fidelity agent-based model along with their lower and upper bounds. Here, t_0 is the time when receiving the tsunami warning (unit: min); n_e is the population; ρ_1 and ρ_3 denote the population proportion on the beach and in the residential area, respectively (the population proportion in the downtown ρ_2 = 1-ρ_1 - ρ_3); p_c is the proportion of the evacuees that use the car; p_f and p_r represent the proportion of the evacuees that follow others and use the official evacuation route, respectively (the proportion of the evacuees that search the shortest path p_s = 1 - p_f - p_r); h_c represents the critical depth (unit: m).

As to outputs (i.e., evacuation performance $y(\mathbf{x}, \xi)$), we consider three types of casualty rates, i.e., pedestrian casualty rate (i.e., number of casualties that evacuate on foot over the population, denoted PCR), car casualty rate (i.e., number of casualties that evacuate by

Table 2. Inputs **x** in the tsunami evacuation simulation using the high-fidelity agent-based model.

x_i	LB	UB	x_i	LB	UB
t_0	3	10	p_c	0	1
τ	0	5	μ_p	1.22	2.68
σ_t	1	5	σ_p	0.05	1
n_e	4000	15,000	p_f	0.1	0.3
ρ_1	0.2	0.6	p_r	0.3	0.6
ρ_3	0.25	0.35	h_c	0.5	2

car over the population, denoted CCR), and total casualty rate (i.e., number of all casualties over the population, denoted TCR). All outputs are collected every 12 time steps in the model, corresponding to 1 minute of the evacuation in actual time. In terms of computational time, depending on the parameters for the simulation (e.g., population size, evacuation modes, etc.), the runtime for each simulation ranges from 2 to 7 hours of CPU time.

4.3.2 *Low-fidelity model*

As discussed in Section 4.2.2, the pedestrian-vehicle interaction and the speed adjustment for both the pedestrian and car are not modeled in the EBM of the low-fidelity agent-based model. Correspondingly, $T_{1_{PA}}$, $T_{2_{PA}}$, $T_{1_{MA}}$, $T_{2_{MA}}$, $T_{1_{Mac}}$, $T_{2_{Mac}}$, $T_{1_{LR}}$, and $T_{2_{LR}}$ are not included in the model parameters ξ compared to the evacuation simulation using the high-fidelity model. As to inputs **x**, a smaller population size will is used by scaling the actual n_e in **x** by one half when building the low-fidelity model. This low-fidelity model is run with a time step of ten seconds with data collected every 6 steps, which again corresponds to 1 minute of the evacuation in actual time. Other details on the evacuation simulation in terms of the inputs and outputs using the low-fidelity model are the same as those using the high-fidelity model. In terms of computational time, depending on the parameters for the simulation, the runtime for each simulation ranges from 0.5 to 1.5 hours of CPU time, corresponding to significant reduction in runtime compared to that for the high-fidelity model.

4.3.3 *MFGP*

For the multi-fidelity training data, $n_h = 50$ and $n_l = 200$ are used. This selection leads to average *ME* below 1% for the interested outputs. For each $\mathbf{x}$ in the training set, to evaluate the corresponding $\mathbf{y}(\mathbf{x})$, which corresponds to the mean of $y(\mathbf{x}, \xi)$ in the current example, 50 simulations are run under 50 realizations of the parameters ξ generated from $p(\xi|\mathbf{x})$. In this study, for the outputs we focus on the TCR and PCR over time and train MFGP models for these outputs. For these outputs, the output dimension is $n_y = 60$. By applying PCA, the dimension can be reduced to around $n_z = 11$ that accounts for more than 99.9% of the total variance in the training data. In the future, outputs with much higher n_y values will be investigated (e.g., when looking at responses over all the 757 patches in the ABM model and over time, the output dimension would be around $n_y = 757 \times 60 = 45420$). In those cases, more significant reductions in the output dimensions by PCA are expected.

5 RESULTS AND DISCUSSIONS

5.1 *Tsunami evacuation risk assessment*

For tsunami evacuation risk assessment, we consider the uncertain input $\mathbf{x}$ with distributions defined in Table 3. For $\mathbf{x}$ that follow truncated normal distribution (denoted TN), "Parameter 1" and "Parameter 2" following the uniform distribution, respectively, represents the mean and SD of the corresponding normal distribution. The $\mathbf{x}$ other than n_e, ρ_1, ρ_3, and p_c follow uniform distribution on the interval between "Parameter 1" and "Parameter 2". We select the mean of the casualty rate (i.e., PCR, CCR, and TCR) over uncertain ξ as the risk consequence measure. Then the evacuation risk corresponds to the expected value of these casualty rates.

Table 3. Distributions of the uncertain inputs $\mathbf{x}$ in the tsunami evacuation simulation.

x_i	Distribution	Parameter 1	Parameter 2
t_0	U	3	10
τ	U	0	5
σ_t	U	1	5
n_e	TN	U[4K, 15K]	U[3K, 7K]
ρ_1	TN	U[0.2, 0.6]	U[0.05, 0.25]
ρ_3	TN	U[0.25, 0.35]	U[0.05, 0.25]
p_c	TN	U[0, 1]	U[0.05, 0.25]
μ_p	U	1.22	2.68
σ_p	U	0.05	1
p_f	U	0.1	0.3
p_r	U	0.3	0.6
h_c	U	0.5	2

Three cases (case 1-3) are investigated to illustrate the efficient tsunami evacuation risk assessment. Case 1 is to estimate the variation of the evacuation risk with time after the earthquake. Previous studies have shown that the proportion of the evacuees that evacuate by car (i.e, p_c) and the population (i.e, n_e) have relatively large impacts on the evacuation risk (Wang and Jia, 2021). To investigate this we define case 2 to estimate the variation of $H(p_c)$ as a function of p_c, and case 3 to estimate the variation of $H(p_c, n_e)$ as a function of $[p_c, n_e]$. For case 2 and 3, the expected casualty rates correspond to the ones at the end of the evacuation simulation (i.e., at t=60 min). The risk for all these cases are estimated using the trained MFGP with N=2000 simulations, which only takes several minutes, corresponding to great efficiency.

5.2 *Results and discussions*

Fig. 4 shows the variation of the evacuation risk with time after the earthquake (i.e., case 1). No casualty occurs till around 29 min after the earthquake when the inundation reaches the community. After around 29 min, casualty starts occurring and all the PCR, CCR, TCR start increasing over time. Overall, both the PCR and CCR first increase slowly before around t=35 min and then increase fast till around t=45 min, after which both the PCR and CCR increase slowly till around t=50 min (when the inundation reaches the run-up limit) and then almost do not increase till the end of the evacuation. The variation of the TCR with time shows a similar trend.

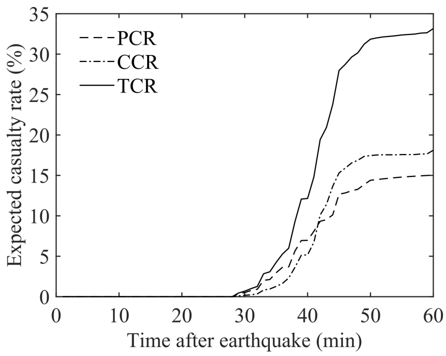

Figure 4. Variation of the evacuation risk with time after the earthquake.

The variation of the expected casualty rate $H(p_c)$ as a function of p_c (i.e., case 2) is shown in Fig. 5. The PCR decreases with an increase of p_c (i.e., more cars and fewer pedestrians), i.e., from 39.7% to 0. This decrease can be attributed to the decrease in the number of pedestrians and less pedestrian congestion due to fewer people evacuating on foot. The CCR increases with the increase of p_c, i.e., from 0 at $p_c = 0$ to 43.2% at $p_c = 1$, which means that the increase of car use would increase the CCR significantly. This can be attributed to the increase in the number of cars or potentially more severe traffic congestion caused by more car uses. Due to the decrease of the PCR and increase of the CCR with p_c, the TCR first decreases (i.e., from 39.7% to 28.5%) and then increases (i.e., from 28.5% to 43.2%). Some value of p_c exists such that the corresponding TCR is minimum, i.e., p_c=0.4 leads to a minimum TCR of 28.5%.

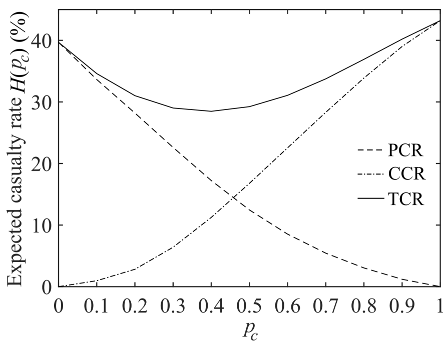

Figure 5. Variation of the expected casualty rate $H(p_c)$ as a function of p_c.

Fig. 6 shows the variation of the expected PCR and CCR as a function of $[p_c, n_e]$. (i.e., case 3). For the PCR under any given value of n_e, it shows a similar trend to that under the uncertain n_e in case 2, i.e., the PCR decreases as p_c increases. Under the given value of p_c, the PCR increases as n_e increases, e.g., the PCR increases from 28.3% when n_e=4000 to 49.1% when n_e=15,000 under p_c=0. This should be attributed to the more severe pedestrian congestion as more people evacuate on foot. Due to the same reason, the increase of the PCR with the increase of n_e is larger under the smaller value of p_c. For the CCR under any given population, it shows a similar trend to that under the uncertain population in case 2, i.e., the CCR increases as p_c increases. In this sense, the variation of the CCR with p_c shows an opposite trend to that for the PCR. However, the variation of the CCR with n_e shows a similar trend to that for the PCR.

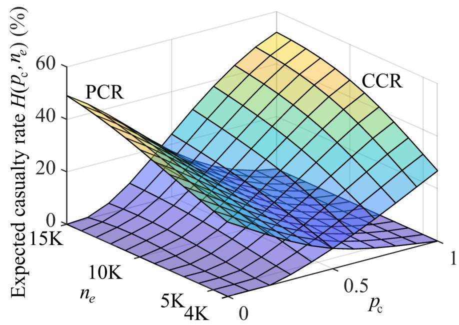

Figure 6. Variation of the expected PCR and CCR as a function of $[p_c, n_e]$.

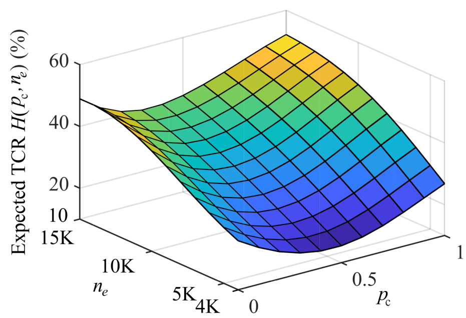

Figure 7. Variation of the expected TCR as a function of $[p_c, n_e]$.

The variation of the expected TCR as a function of $[p_c, n_e]$. (i.e., case 3) is shown in Fig. 7. Under any given population, the TCR first decreases and then increases with the car use (i.e., p_c). This variation of the TCR with p_c is consistent with that in case

2 corresponding to uncertain n_e. However, the value of p_c corresponding to the minimum TCR is smaller under a larger population. Under any given value of p_c, the TCR increases significantly with n_e, which means the evacuation risk would be higher for a larger population.

6 CONCLUSIONS

This paper proposed to use multi-fidelity Gaussian process (GP) surrogate model to replace the high-fidelity ABM model for efficient evacuation risk assessment. To train the MFGP, ABM models with different fidelity levels and computational efforts were established. PCA was integrated with MFGP to facilitate training of MFGP models for high-dimensional outputs. The trained MFGP model was used to efficiently evaluate the tsunami evacuation risk for Seaside, Oregon. The results verified the high efficiency of the MFGP model in evacuation risk assessment.

7 ACKNOWLEDGMENT

This research is supported in part by the National Science Foundation Engineering Design and System Engineering Program under grant number CMMI-2034040. This support is gratefully acknowledged.

REFERENCES

Bonabeau, E. (2002). "Agent-based modeling: Methods and techniques for simulating human systems." *Proceedings of the National Academy of Sciences*, Vol. 99, Irvine, CA, 7280–7287.

Dubourg, V., Sudret, B., and Bourinet, J.-M. (2011). "Reliability-based design optimization using kriging surrogates and subset simulation." *Structural and Multidisciplinary Optimization*, 44(5), 673–690.

Gidaris, I., Taflanidis, A. A., and Mavroeidis, G. P. (2015). "Kriging metamodeling in seismic risk assessment based on stochastic ground motion models." *Earthquake Engineering & Structural Dynamics*, 44, 2377–2399.

Jia, G. and Taflanidis, A. A. (2013). "Kriging metamodeling for approximation of high-dimensional wave and surge responses in real-time storm/hurricane risk assessment." *Computer Methods in Applied Mechanics and Engineering*, 261, 24–38.

Jia, G., Taflanidis, A. A., Nadal-Caraballo, N. C., Melby, J. A., Kennedy, A. B., and Smith, J. M. (2016). "Surrogate modeling for peak or time-dependent storm surge prediction over an extended coastal region using an existing database of synthetic storms." *Natural Hazards*, 81(2), 909–938.

Kennedy, M. C. and O'Hagan, A. (2000). "Predicting the output from a complex computer code when fast approximations are available." *Biometrika*, 87(1), 1–13.

Li, M. and Jia, G. (2020). "Multifidelity gaussian process model integrating low-and high-fidelity data considering censoring." *Journal of Structural Engineering*, 146(3), 04019215.

Mostafizi, A., Wang, H., Cox, D., Cramer, L. A., and Dong, S. (2017). "Agent-based tsunami evacuation modeling of unplanned network disruptions for evidence-driven resource allocation and retrofitting strategies." *Natural Hazards*, 88(3), 1347–1372.

Mostafizi, A., Wang, H., Cox, D., and Dong, S. (2019). "An agent-based vertical evacuation model for a near-field tsunami: Choice behavior, logical shelter locations, and life safety." *International Journal of Disaster Risk Reduction*, 34, 467–479.

Qian, Z., Seepersad, C. C., Joseph, V. R., Allen, J. K., and Wu, C. J. (2006). "Building surrogate models based on detailed and approximate simulations." *Journal of Mechanical Design*, 128(4), 668–677.

USGS (2020). "Cascadia Subduction Zone. Retrieved from https://www.usgs.gov/media/images/cascadia-subduction-zone-1.

Wang, H., Mostafizi, A., Cramer, L. A., Cox, D., and Park, H. (2016). "An agent-based model of a multimodal near-field tsunami evacuation: Decision-making and life safety." *Transportation Research Part C: Emerging Technologies*, 64, 86–100.

Wang, Z. (2021). "Simulation-based tsunami evacuation risk assessment and risk-informed mitigation." Ph.D. thesis, Colorado State University, Colorado State University.

Wang, Z. and Jia, G. (2021). "A novel agent-based model for tsunami evacuation simulation and risk assessment." *Natural Hazards*, 105(2), 2045–2071.